Available online at www.sciencedirect.com
ScienceDirect
Journal of Computational Physics 224 (2007) 663–680
JOURNAL OF COMPUTATIONAL PHYSICS
www.elsevier.com/locate/jcp

A rapid boundary integral equation technique for protein electrostatics

Scott Grandison [a], Robert Penfold [b,*], Jean-Marc Vanden-Broeck [a]

[a] School of Mathematics, University of East Anglia, Norwich NR4 7TJ, UK
[b] Institute of Food Research, Food Materials Division, Norwich Research Park, Colney, Norwich, NORFOLK NR4 7UA, UK

Received 20 April 2006; received in revised form 20 September 2006; accepted 14 October 2006
Available online 28 November 2006

Abstract

A new boundary integral formulation is proposed for the solution of electrostatic field problems involving piecewise uniform dielectric continua. Direct Coulomb contributions to the total potential are treated exactly and Green's theorem is applied only to the residual reaction field generated by surface polarisation charge induced at dielectric boundaries. The implementation shows significantly improved numerical stability over alternative schemes involving the total field or its surface normal derivatives. Although strictly respecting the electrostatic boundary conditions, the partitioned scheme does introduce a jump artefact at the interface. Comparison against analytic results in canonical geometries, however, demonstrates that simple interpolation near the boundary is a cheap and effective way to circumvent this characteristic in typical applications. The new scheme is tested in a naive model to successfully predict the ground state orientation of biomolecular aggregates comprising the soybean storage protein, glycinin.
© 2006 Elsevier Inc. All rights reserved.

MSC: 65N38; 78A70; 92C05; 82B21

PACS: 41.20.Cv; 87.50.Rr; 36.20.−r; 87.15.−v

Keywords: Electrostatics; Boundary integral method; Monte Carlo simulation; Biomolecular interactions

1. Introduction

A consensus has now emerged maintaining that the structure, properties, behaviour and function of many biomolecules, including proteins [1] and nucleic acids [2], are often controlled by electrostatic (Coulomb) interactions. Consequently, mathematical models for aqueous biomolecular solutions consisting of point charge distributions in piecewise uniform dielectric continua are believed to capture much of the basic physics relevant for important biological phenomena. In equilibrium, small mobile charges representing counterions and

* Corresponding author. Tel.: +44 1603 25 5156; fax: +44 1603 50 7723.
E-mail addresses: s.grandison@uea.ac.uk (S. Grandison), robert.penfold@bbsrc.ac.uk (R. Penfold), j.vanden-broeck@uea.ac.uk (J.-M. Vanden-Broeck).

0021-9991/$ - see front matter © 2006 Elsevier Inc. All rights reserved.
doi:10.1016/j.jcp.2006.10.021

dissolved salts are typically treated by invoking an approximate thermal distribution (Poisson–Boltzmann (PB) equation), very often at the level of linear response (Debye–Hückel (DH) theory). Although full space finite difference methods first appeared for analysing such models [3–5], modern finite element techniques with multi-level adaptive mesh refinement [6] provide significantly improved resolution and superior complexity scaling for large systems. Alternatively, the implementation of boundary element (BE) formulations offer several important advantages [7] including lower dimensionality, respect for far-field constraints, precise interface representation with exactly enforced boundary conditions, and the off-lattice realisation of electrostatic fields. For biomolecular models, perhaps the most appealing aspect of the BE method is the natural and straightforward extension to multiple domains defined by disjoint boundaries. Hitherto this feature has received scant attention beyond the early work of Zhou [8] where the interaction energy of yeast cytochrome *c* and its electron-transfer partner (yeast cytochrome *c* peroxidase) was calculated using the BE method within the PB approximation. Despite some technical difficulties associated with moving boundaries, it seems that the utility of BE methods remains to be fully realised for the study of all manner of macromolecular interactions including enzyme-substrate docking, nucleic acid binding, protein gelation and amyloid formation. In this preliminary work, we aim to demonstrate the promise of BE methods in such applications by considering the athermal ground state configuration of a homohexamer formed from glycinin subunits that are members of the 11S globulin family of storage proteins common to most plant seeds [9].

Early "indirect" BE methods [10,11] expressed the total electrostatic potential Φ as a surface integral of either the single- or double-layer induced polarisation contributions and solved for the unknown surface density. These approaches are especially well suited for engineering applications involving highly heterogeneous composite materials; in the design of electric devices and high voltage systems, for example, or for non-destructive testing. "Direct" methods [12,13], that invoke Green's theorem to recast the governing Maxwellian partial differential equation as an integral equation in Φ, can accommodate non-zero ionic strength in the aqueous domain and therefore appear most appropriate for biomolecular models. Moreover, the "derivative" formulation [14,7] explicitly appeals to continuity of the displacement field at the boundary to form a discrete integral equation with superior numerical stability. Within the DH linear response framework, Lu et al. [15] have recently formulated two independent direct BE methods making use of a variational principle in the first instance [15a], or alternatively applying the hypersingular integral technique [15b] to calculate the Maxwell stress tensor on the dielectric boundary. Both approaches yield the effective DH interaction energies and forces suitable for Brownian dynamics simulation of biomolecular association processes.

In this paper, we report on the detailed implementation of a direct, non-derivative BE method that departs from previous work in two ways. First, the statistical mechanical problem, of estimating macroscopic observables of a many-body fluid system at thermal equilibrium, is divorced from the electrostatic problem of evaluating the energy of a *fixed* charge array. By exploiting the computational efficiency of the BE method, macromolecular solute charges and ions dissolved in the aqueous phase are both treated consistently without discrimination [16]. Given the electrostatic energy of any fixed configuration, thermal averages or dynamical information can be recovered by appropriate simulation techniques: either by constructing a Markovian sample of states from the equilibrium ensemble (Monte Carlo) [16]; or by numerically integrating the equation of motion (molecular dynamics). The second innovation concerns the boundary integral equation itself, which is reformulated in terms of the *reaction* field alone, instead of the total potential. Although this increases storage requirements, numerical stability is significantly enhanced even for crude interface representations. Furthermore, because the reaction field satisfies the Laplace equation everywhere, this approach facilitates calculation of the Maxwell stress tensor at any point on the dielectric interface [15b]. A novel and successful treatment of surface singularities is also described, that may be of particular value in reaction field methods for electronic structure calculations of solute properties [17].

As a prelude to the development of general but necessarily numerical BE methods, we are interested in heuristic canonical geometries (infinite plane, sphere and infinite right circular cylinder) where a good deal of analytic progress can be made. These results will form a test-bed for comprehensively evaluating the performance of the BE implementation. Standard solutions in the plane geometry are often interpreted with the idea of "image" charges: virtual point singularities in a completely uniform dielectric that generate exactly equivalent potential fields that would arise from actual surface charge distributions induced on discontinuous dielectric boundaries. Although the corresponding treatments for two parallel planes [18] and for the sphere [19] yield an

infinite series of images, the notion remains appealing and physically helpful. Indeed, the convergent "multiple induction expansion" developed by Shaw [20] can be regarded as a formal demonstration that the image charge concept is quite general. After some rudimentary remarks, the following Section 2 explicitly exhibits an image charge series for the circular cylindrical case, relevant for simple models of linear polyelectrolytes and nucleic acids, before going on to describe the new BE formulation. Details of the numerical implementation are explained in Section 3, while test results and the glycinin application are considered in Section 4. Section 5 concludes the paper with a general discussion and summary comments.

2. Formulation

2.1. Rudimentary considerations

Define an open "interior" domain $\mathscr{D} \subseteq \mathbb{R}^3$ that contains a single point charge q located at $\mathbf{r}_q \in \mathscr{D}$ and that is distinguished from an adjacent, open and charge free "exterior" domain $\overline{\mathscr{D}}$ by the continuous and smooth boundary Γ such that $\mathscr{D} \cup \Gamma \cup \overline{\mathscr{D}} = \mathbb{R}^3$ while all the sets are mutually disjoint. Both domains are supposed to comprise of a homogeneous, isotropic and linear continuum material so that their electric response is completely characterised by the scalar relative permittivities ε^{int} and ε^{ext}, respectively. The total electrostatic potential field (or Green function) on each domain can be written,

$$\Phi^{\text{int}}(\mathbf{r}) = \phi_{\text{C}}^{\text{int}}(\mathbf{r}) + \psi^{\text{int}}(\mathbf{r}) \quad (\mathbf{r} \in \mathscr{D}), \tag{1}$$

$$\Phi^{\text{ext}}(\mathbf{r}) = \psi^{\text{ext}}(\mathbf{r}) \quad (\mathbf{r} \in \overline{\mathscr{D}}) \tag{2}$$

with a Coulomb contribution arising as a solution of the Poisson equation,

$$\nabla^2 \phi_{\text{C}}^{\text{int}}(\mathbf{r}) = -\frac{q}{\epsilon_0 \varepsilon^{\text{int}}} \delta(\mathbf{r} - \mathbf{r}_q), \tag{3}$$

where ϵ_0 is the vacuum permittivity, and a "reaction" field that satisfies the Laplace equation everywhere,

$$\nabla^2 \psi^{\text{int}}(\mathbf{r}) = \nabla^2 \psi^{\text{ext}}(\mathbf{r}) = 0. \tag{4}$$

Together with the boundary conditions on the normal component of the dielectric displacement field (electric flux density) and the tangential components of the electric field,

$$\begin{aligned} &\varepsilon^{\text{ext}} \nabla \Phi^{\text{ext}}(\mathbf{r}) - \varepsilon^{\text{int}} \nabla \Phi^{\text{int}}(\mathbf{r})\big) \cdot \mathbf{n} = 0 \\ &\nabla \Phi^{\text{ext}}(\mathbf{r}) - \nabla \Phi^{\text{int}}(\mathbf{r})\big) \times \mathbf{n} = 0 \end{aligned} \quad (\mathbf{r} \in \Gamma), \tag{5}$$

explicit expressions for Φ can be obtained if the surface Γ (with unit normal $\mathbf{n}$ directed from the interior to the exterior domains) is simply parametrised in coordinate systems where the Laplacian operator is separable. In particular, we consider an infinite flat plane, a sphere and an infinite circular cylinder.

2.1.1. Plane boundary Γ

In a cylindrical coordinate system (ρ, φ, z), define the boundary Γ: $z = 0$ and let the interior domain correspond to the half-space $z > 0$ with the point charge q situated at $(0, 0, d)$ for $d > 0$ (see Fig. 1(a)). By virtue of the polar symmetry, we have $\Phi = \Phi(\rho, z)$ and Maxwell's equations can be solved by the method of images [21] to obtain,

$$\phi_{\text{C}}^{\text{int}}(\rho, z) = \frac{q}{4\pi\epsilon_0 \varepsilon^{\text{int}}} (\rho^2 + (z - d)^2)^{-1/2}, \tag{6}$$

$$\psi^{\text{int}}(\rho, z) = -\frac{q\Upsilon_\varepsilon}{4\pi\epsilon_0 \varepsilon^{\text{int}}} (\rho^2 + (z + d)^2)^{-1/2} = \frac{Q}{4\pi\epsilon_0 \varepsilon^{\text{int}}} (\rho^2 + (z - R)^2)^{-1/2}, \tag{7}$$

$$\psi^{\text{ext}}(\rho, z) = \frac{q}{4\pi\epsilon_0 \bar{\varepsilon}} (\rho^2 + (z - d)^2)^{-1/2}, \tag{8}$$

where

$$\Upsilon_\varepsilon = \frac{\varepsilon^{\text{ext}} - \varepsilon^{\text{int}}}{\varepsilon^{\text{ext}} + \varepsilon^{\text{int}}} \quad \text{such that } |\Upsilon_\varepsilon| < 1 \quad \text{and} \quad \bar{\varepsilon} = \frac{\varepsilon^{\text{ext}} + \varepsilon^{\text{int}}}{2}.$$

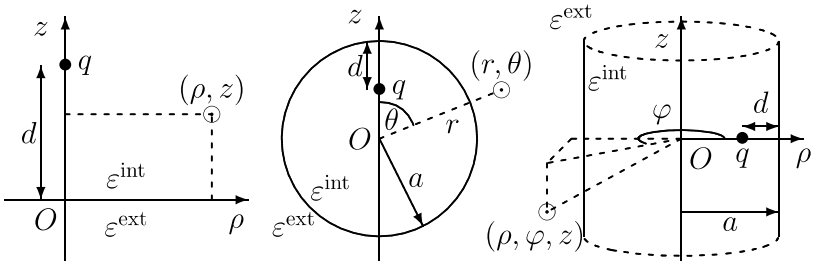

(a) Planar (b) Spherical (c) Cylindrical

Fig. 1. Sketches defining geometric parameters for simple dielectric boundaries. A point charge q is located a distance d from a dielectric interface that distinguishes continua of relative permittivity ε^{int} and ε^{ext}. (a) Planar, (b) spherical, (c) cylindrical.

The internal reaction field ψ^{int} can be strictly regarded as a Coulomb interaction with a point "image" charge $Q = -q\Upsilon_\varepsilon$ situated at $(0,0,R) = (0,0,-d)$. Similarly, the external reaction field ψ^{ext} is just a Coulomb interaction with the free charge q, but screened by an "average" continuum characterised by the dielectric constant $\bar{\varepsilon}$.

2.1.2. Spherical boundary Γ

In a spherical polar coordinate system (r,θ,φ), define the boundary $\Gamma : r = a$ and let the interior domain correspond to $r < a$ with the point charge q situated at $(a-d,0,0)$ for $0 < d \leqslant a$ (see Fig. 1(b)). By virtue of the azimuthal symmetry, we have $\Phi = \Phi(r,\theta)$, while the finite extent of the surface imposes a discrete spectrum of modes so that the Legendre polynomials P_n provide a complete orthogonal basis to expand the Green functions [19,22,23],

$$\phi_{\text{C}}^{\text{int}}(r,\theta) = \frac{q}{4\pi\epsilon_0\varepsilon^{\text{int}}}\frac{1}{r_>}\sum_{n=0}^{\infty}\left(\frac{r_<}{r_>}\right)^n P_n(\cos\theta), \tag{9}$$

$$\psi^{\text{int}}(r,\theta) = -\frac{q\Upsilon_\varepsilon}{4\pi\epsilon_0\varepsilon^{\text{int}}}\frac{1}{a}\sum_{p=0}^{\infty}\left(\frac{1-\Upsilon_\varepsilon}{2}\right)^p\sum_{n=0}^{\infty}(n+1)^{-p}\left(\frac{r}{a/(1-d/a)}\right)^n P_n(\cos\theta) = \sum_{p=0}^{\infty}\psi_p^{\text{int}}(r,\theta), \tag{10}$$

$$\psi^{\text{ext}}(r,\theta) = \frac{q}{4\pi\epsilon_0\bar{\varepsilon}}\frac{1}{r}\sum_{p=0}^{\infty}(-\Upsilon_\varepsilon)^p\sum_{n=0}^{\infty}(2n+1)^{-p}\left(\frac{a-d}{r}\right)^n P_n(\cos\theta) = \sum_{p=0}^{\infty}\psi_p^{\text{ext}}(r,\theta), \tag{11}$$

where $r_< = \min\{r, a-d\}$ and $r_> = \max\{r, a-d\}$. To lowest order in the geometric series over p we have,

$$\psi_0^{\text{int}}(r,\theta) = \frac{Q}{4\pi\epsilon_0\varepsilon^{\text{int}}}\frac{1}{R}\sum_{n=0}^{\infty}\left(\frac{r}{R}\right)^n P_n(\cos\theta), \tag{12}$$

$$\psi_0^{\text{ext}}(r,\theta) = \frac{q}{4\pi\epsilon_0\bar{\varepsilon}}\frac{1}{r}\sum_{n=0}^{\infty}\left(\frac{a-d}{r}\right)^n P_n(\cos\theta) \tag{13}$$

with $Q = -q\Upsilon_\varepsilon/(1-d/a)$ and $R = a/(1-d/a)$. In analogy with the planar case, we again recognise ψ_0^{int} as a Coulomb interaction arising from a modulated image charge Q situated at $(R,0,0)$ in the exterior domain, while ψ_0^{ext} is just a direct Coulomb field in a transformed continuum with relative permittivity $\bar{\varepsilon}$.

2.1.3. Circular cylindrical boundary Γ

In a circular cylindrical coordinate system (ρ,φ,z), let $\Gamma : \rho = a$ define the boundary with the interior domain corresponding to $\rho < a$ and the point charge q situated at $(a-d,0,0)$ for $0 < d \leqslant a$ (see Fig. 1(c)). The unlimited extent of the surface parallel to the cylinder axis supports a continuous spectrum, while for the bounded radial coordinate, the product of modified Bessel functions I_m (first kind, regular at the origin) and K_m (second kind, regular at infinity) provides a suitable basis of discrete modes to expand the solutions. Following Hochberg et al. [24], we get,

$$\phi_{\mathrm{C}}^{\mathrm{int}}(\rho,\varphi,z)=\frac{q}{\pi^2\epsilon_0\varepsilon^{\mathrm{int}}}\frac{1}{\rho_>}\sum_{m=0}^{\infty}\frac{\cos(m\varphi)}{1+\delta_{m0}}\int_0^{\infty}\mathrm{d}\xi\,\cos(\xi z/\rho_>)I_m(\xi\rho_</\rho_>)K_m(\xi), \tag{14}$$

$$\psi^{\mathrm{int}}(\rho,\varphi,z)=-\frac{q\Upsilon_\varepsilon}{\pi^2\epsilon_0\varepsilon^{\mathrm{int}}}\frac{1}{a}\sum_{p=0}^{\infty}\left(\frac{1-\Upsilon_\varepsilon}{2}\right)^p\sum_{m=0}^{\infty}\frac{\cos(m\varphi)}{1+\delta_{m0}}\int_0^{\infty}\mathrm{d}\xi\,(N_m(\xi)+1)^{-p}$$
$$\times\cos(\xi z/a)\left(\frac{I_m(\xi(1-d/a))I_m(\xi\rho/a)}{I_m(\xi)}\right)K_m(\xi)=\sum_{p=0}^{\infty}\psi_p^{\mathrm{int}}(\rho,\varphi,z), \tag{15}$$

$$\psi^{\mathrm{ext}}(\rho,\varphi,z)=\frac{q}{\pi^2\epsilon_0\bar{\varepsilon}}\frac{1}{\rho}\sum_{p=0}^{\infty}(-\Upsilon_\varepsilon)^p\sum_{m=0}^{\infty}\frac{\cos(m\varphi)}{1+\delta_{m0}}\int_0^{\infty}\mathrm{d}\xi\,(2N_m(\xi d/\rho)+1)^{-p}$$
$$\times\cos(\xi z/\rho)I_m(\xi(a-d)/\rho)K_m(\xi)=\sum_{p=0}^{\infty}\psi_p^{\mathrm{ext}}(\rho,\varphi,z), \tag{16}$$

where $\rho_<=\min\{\rho,a-d\}$ and $\rho_>=\max\{\rho,a-d\}$, with Kronecker's δ_{ij} and,

$$N_m(t)=\frac{U_m(t)}{1-U_m(t)}>0\quad\text{with } U_m(t)=\left|\frac{I_m'(t)K_m(t)}{I_m(t)K_m'(t)}\right|<1. \tag{17}$$

The restriction on U_m follows from the strictly monotonic decreasing character of the product $I_\nu(t)K_\nu(t)$ for all real order $\nu\geqslant 0$ and non-negative real argument t [25]. Given $\rho<a$, making use of the inequality demonstrated by Joshi and Bissu [26],

$$\exp(-\lambda\xi(1-\rho/a))\left(\frac{\rho}{a}\right)^m<\frac{I_m(\lambda\xi\rho/a)}{I_m(\lambda\xi)}<\left(\frac{\rho}{a}\right)^m, \tag{18}$$

where $\lambda=1-d/a$, and further considering the situation $d\ll a$ with $\rho\simeq a$, we have,

$$\frac{I_m(\xi(1-d/a))I_m(\xi\rho/a)}{I_m(\xi)}\approx I_m\left(\xi\frac{\rho}{a/(1-d/a)}\right). \tag{19}$$

Substitution in (15) yields to lowest order in the geometric series over p,

$$\psi_0^{\mathrm{int}}(\rho,\varphi,z)=\frac{Q}{\pi^2\epsilon_0\varepsilon^{\mathrm{int}}}\frac{1}{R}\sum_{m=0}^{\infty}\frac{\cos(m\varphi)}{1+\delta_{m0}}\int_0^{\infty}\mathrm{d}\xi\,\cos(\xi z/R)I_m(\xi\rho/R)K_m(\xi), \tag{20}$$

$$\psi_0^{\mathrm{ext}}(\rho,\varphi,z)=\frac{q}{\pi^2\epsilon_0\bar{\varepsilon}}\frac{1}{\rho}\sum_{m=0}^{\infty}\frac{\cos(m\varphi)}{1+\delta_{m0}}\int_0^{\infty}\mathrm{d}\xi\,\cos(\xi z/\rho)I_m(\xi(a-d)/\rho)K_m(\xi) \tag{21}$$

with $Q=-q\Upsilon_\varepsilon/(1-d/a)$ and $R=a/(1-d/a)$, as before. Again, ψ_0^{int} appears as a Coulomb field from the point source Q situated at $(R,0,0)$, while ψ_0^{ext} is just a direct Coulomb interaction from the charge q but in an average dielectric continuum.

2.1.4. General remarks

Although only a single charge is considered here, non-zero work is nevertheless required to assemble the system since the dielectric inhomogeneity is polarised by the ion field and, in turn, generates a potential ψ^{int} that couples with the charge [27]. This polarisation energy is just,

$$\Delta U^{\mathrm{int}}=\frac{1}{2}q\psi^{\mathrm{int}}(\mathbf{r}_q). \tag{22}$$

Each of the canonical boundary geometries, in coordinate systems where the Laplacian is separable, exhibit a Green function with essentially the same structure. Interpretation of the reaction field in terms of a finite number of point "image" sources is exact only for the plane boundary case, but does provide a useful conceptual framework for analysing the leading order induced polarisation charge contributions from boundaries with curvature. The similarities suggest an approximate general description as follows. An infinitesimal test charge (of opposite polarity to q) placed in $\mathscr{D}$ will experience an attractive Coulomb force from the free charge as well as a weaker central force originating from $\overline{\mathscr{D}}$ that may be attractive ($\varepsilon^{\mathrm{int}}>\varepsilon^{\mathrm{ext}}\Rightarrow -1<\Upsilon_\varepsilon<0$) or repulsive

($\varepsilon^{\text{int}} < \varepsilon^{\text{ext}} \Rightarrow 0 < \Upsilon_\varepsilon < 1$) depending on the relative dielectric response of the two media. The additional force stems from a charge distribution *induced* at the surface as a result of inhomogeneous polarisation in the presence of the electric field generated by q, and is therefore sensitive to the proximity d of $\mathbf{r}_q$ to Γ. A similar test charge placed in the exterior domain $\overline{\mathscr{D}}$ will be subject to an always attractive force that can be interpreted as a direct Coulombic charge–charge interaction with the source q, but screened by an "average" continuum. The magnitude of this force is again governed by the mismatch of dielectric response and may be smaller ($-1 < \Upsilon_\varepsilon < 0$) or larger ($0 < \Upsilon_\varepsilon < 1$) than a corresponding free charge–charge interaction at the same separation but entirely within the exterior domain. With this interpretation, the effect of surface induced polarisation charge on the external fields is to simply re-scale the dielectric response in a manner that is decoupled from the proximity d. In the primitive model ($\varepsilon^{\text{int}} = \varepsilon^{\text{ext}} = \bar{\varepsilon} = \varepsilon \Rightarrow \Upsilon_\varepsilon = 0$), the internal reaction field vanishes while, in accord with the interpretation above, ψ^{ext} becomes a smooth extension of the Coulomb field into the exterior domain, with a form identical to $\phi_{\text{C}}^{\text{int}}$ as we should expect.

2.2. Boundary integral method

Throughout the following development, lengths and energies are rendered non-dimensional by scaling with Bjerrum and thermal units, respectively. Thus, spatial positions $\mathbf{r}$ and electrostatic potential energies $q\Phi$ become,

$$\frac{\epsilon_0 kT\mathbf{r}}{q^2} \leftrightarrow \mathbf{r} \quad \text{and} \quad \frac{q\Phi}{kT} \leftrightarrow \Phi,$$

where q is the elementary charge unit (of a proton), k is the Boltzmann constant and T is the absolute temperature.

Consider an open three dimensional domain $\mathscr{D} \subseteq \mathbb{R}^3$ of linear, isotropic dielectric material with relative permittivity ε^{int}, bounded by a smooth, closed surface Γ and containing N^{int} point ions, each with valency ζ_i and located at $\mathbf{r}_i$ for $i = 1, \ldots, N^{\text{int}}$. The Poisson equation then reads,

$$\nabla^2 \Phi^{\text{int}}(\mathbf{r}) = -\frac{1}{\varepsilon^{\text{int}}} \sum_{i=1}^{N^{\text{int}}} \zeta_i \delta(\mathbf{r} - \mathbf{r}_i) \quad (\mathbf{r} \in \mathscr{D}) \tag{23}$$

and the corresponding general solution (Green function) for the electric potential field Φ is obtained as

$$\Phi^{\text{int}}(\mathbf{r}) = \phi_{\text{C}}^{\text{int}}(\mathbf{r}) + \psi^{\text{int}}(\mathbf{r}) = \begin{cases} \frac{1}{4\pi\varepsilon^{\text{int}}} \sum_{i=1}^{N^{\text{int}}} \frac{\zeta_i}{|\mathbf{r}-\mathbf{r}_i|} + \psi^{\text{int}}(\mathbf{r}) & (\mathbf{r} \in \mathscr{D} \cup \Gamma), \\ 0 & (\mathbf{r} \in \overline{\mathscr{D}}). \end{cases} \tag{24}$$

The auxiliary potential ψ can be chosen to accommodate external boundary conditions on Γ, but must satisfy the Laplace equation within the domain,

$$\nabla^2 \psi^{\text{int}}(\mathbf{r}) = 0 \quad (\mathbf{r} \in \mathscr{D} \cup \Gamma), \qquad \psi^{\text{int}}(\mathbf{r}) = 0 \quad (\mathbf{r} \in \overline{\mathscr{D}}). \tag{25}$$

In physical terms, this so-called "reaction" field [27] represents the combined contribution from external electrostatic forces directly and from the surface charge density induced on Γ by a discontinuity of the continuum polarisation in the presence of an electric field generated from both internal and external sources. Thus, ψ assumes the role of the "image" field discussed in Section 2.1.

To complete the simple continuum model of a bio-macromolecule in aqueous solution (see Fig. 2), suppose that the complementary domain $\overline{\mathscr{D}}$ is an infinite, uniform dielectric medium of relative permittivity ε^{ext} that may also contain a number N^{ext} of point charges each with valency ζ'_j and located at $\mathbf{r}'_j$ for $j = 1, \ldots, N^{\text{ext}}$. Similarly, the total external potential and reaction field are defined

$$\Phi^{\text{ext}}(\mathbf{r}) = \phi_{\text{C}}^{\text{ext}}(\mathbf{r}) + \psi^{\text{ext}}(\mathbf{r}) = \begin{cases} \frac{1}{4\pi\varepsilon^{\text{ext}}} \sum_{j=1}^{N^{\text{ext}}} \frac{\zeta'_j}{|\mathbf{r}-\mathbf{r}'_j|} + \psi^{\text{ext}}(\mathbf{r}) & (\mathbf{r} \in \overline{\mathscr{D}} \cup \Gamma), \\ 0 & (\mathbf{r} \in \mathscr{D}), \end{cases} \tag{26}$$

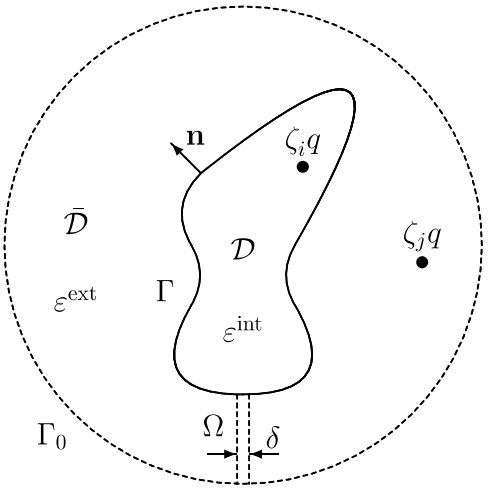

Fig. 2. A schematic diagram of the continuum dielectric model for bio-macromolecular solvation. A bounded dielectric domain $\mathscr{D}$ of permittivity ε^{int} contains charges $\zeta_i q$ and is separated from its complementary region $\overline{\mathscr{D}}$ (with permittivity ε^{ext} and charges $\zeta_j q$) by a smooth interface Γ with unit normal vector $\mathbf{n}$. A narrow cylindrical pipe Ω of diameter δ connects the contour at infinity Γ_0 with the surface Γ.

where

$$\nabla^2\psi^{\text{ext}}(\mathbf{r}) = 0 \quad (\mathbf{r} \in \overline{\mathscr{D}} \cup \Gamma), \qquad \psi^{\text{ext}}(\mathbf{r}) = 0 \quad (\mathbf{r} \in \mathscr{D}). \tag{27}$$

By appealing to the electrostatic boundary conditions,

$$\begin{aligned} &\Phi^{\text{int}}(\mathbf{r}^*) = \Phi^{\text{ext}}(\mathbf{r}^*) \\ &\varepsilon^{\text{int}}\nabla\Phi^{\text{int}}(\mathbf{r}^*)\cdot\mathbf{n} = \varepsilon^{\text{ext}}\nabla\Phi^{\text{ext}}(\mathbf{r}^*)\cdot\mathbf{n} \end{aligned} \quad (\mathbf{r}^* \in \Gamma), \tag{28}$$

a pair of equations are obtained, linear in values of the unknown reaction fields and their normal derivatives on Γ,

$$\begin{aligned} &\psi^{\text{int}}(\mathbf{r}^*) - \psi^{\text{ext}}(\mathbf{r}^*) + \ \phi_{\text{C}}^{\text{int}}(\mathbf{r}^*) - \phi_{\text{C}}^{\text{ext}}(\mathbf{r}^*)\big) = 0 \\ &\varepsilon^{\text{int}}\nabla\psi^{\text{int}}(\mathbf{r}^*) - \varepsilon^{\text{ext}}\nabla\psi^{\text{ext}}(\mathbf{r}^*) + \nabla\ \varepsilon^{\text{int}}\phi_{\text{C}}^{\text{int}}(\mathbf{r}^*) - \varepsilon^{\text{ext}}\phi_{\text{C}}^{\text{ext}}(\mathbf{r}^*)\big)\big)\cdot\mathbf{n} = 0 \end{aligned} \quad (\mathbf{r}^* \in \Gamma), \tag{29}$$

where $\mathbf{n} = \mathbf{n}(\mathbf{r}^*)$ is the unit surface normal directed from the internal region $\mathscr{D}$ to the external domain $\overline{\mathscr{D}}$ (see Fig. 2).

Together with series expansions in a suitable basis set, Eq. (29) are sufficient to analytically calculate the electrostatic potential in cases where Γ has a simple parametric geometry. In particular, Kirkwood [28] obtained a solution for a single spherical boundary that was later extended by Zhou [29] for two disjoint spheres. An arbitrary boundary will generally require numerical methods. Following the "non-derivative" approach described by Liang and Subramaniam [14], Green's second identity furnishes another independent pair of integral equations by making use of the contour Γ_0 at infinity, that is assumed beyond the range of any fields, to obtain in the limit $\delta \to 0$ (see Fig. 2)

$$\psi^{\text{int}}(\mathbf{r}) + \frac{1+\chi(\mathbf{r})}{4\pi}\oint\!\!\!\!\!\!\diagup_{\Gamma} \mathrm{d}\Gamma\left(\psi^{\text{int}}(\mathbf{s})\nabla\left(\frac{1}{|\mathbf{r}-\mathbf{s}|}\right) - \frac{1}{|\mathbf{r}-\mathbf{s}|}\nabla\psi^{\text{int}}(\mathbf{s})\right)\cdot\mathbf{n} = 0 \quad (\mathbf{s} \in \Gamma), \tag{30}$$

$$\psi^{\text{ext}}(\mathbf{r}) - \frac{1+\chi(\mathbf{r})}{4\pi}\oint\!\!\!\!\!\!\diagup_{\Gamma} \mathrm{d}\Gamma\left(\psi^{\text{ext}}(\mathbf{s})\nabla\left(\frac{1}{|\mathbf{r}-\mathbf{s}|}\right) - \frac{1}{|\mathbf{r}-\mathbf{s}|}\nabla\psi^{\text{ext}}(\mathbf{s})\right)\cdot\mathbf{n} = 0 \quad (\mathbf{s} \in \Gamma), \tag{31}$$

where the surface characteristic function is

$$\chi(\mathbf{r}) = \begin{cases} 1 & (\mathbf{r} = \mathbf{r}^* \in \Gamma) \\ 0 & (\mathbf{r} \notin \Gamma) \end{cases}, \tag{32}$$

and the integrals are of principal-value type. The equation system (29)–(31) is closed with respect to the four unknown fields $(\psi^{\text{int}}, \psi^{\text{ext}}, \partial\psi^{\text{int}}/\partial n, \partial\psi^{\text{ext}}/\partial n)$ evaluated on the boundary. Once determined, these can be used subsequently in Eqs. (30) and (31) to calculate the total potential anywhere.

3. Implementation

3.1. Singularities

Clearly, evaluating the boundary integrals for field points on the surface $\mathbf{r} = \mathbf{r}^*$ will encounter singularities at $\mathbf{s} = \mathbf{r}^*$. Moreover, practical calculations are typically carried out on an approximate discrete mesh containing non-analytic vertices and edges. Normal derivatives of quantities can only be estimated at a vertex, for example, by taking averages over the adjacent faces. In general this method does not yield accurate results so that such derivatives should be computed over faces while taking appropriate measures to account for the singularity that occurs. The approach described here is similar to the technique of Parau and Vanden-Broeck [30], though the singular integral obtained is calculated in a different manner.

For either reaction field ($\alpha = \{\text{int}, \text{ext}\}$), the offending singularity is first isolated into a term that depends only on the boundary geometry, thus,

$$\begin{aligned}\psi^{\alpha}(\mathbf{r}^*) \pm \frac{1}{2\pi} \oiint_{\Gamma} \mathrm{d}\Gamma \left(\psi^{\alpha}(\mathbf{s}) \nabla \left(\frac{1}{|\mathbf{r}^* - \mathbf{s}|} \right) - \frac{1}{|\mathbf{r}^* - \mathbf{s}|} \nabla (\psi^{\alpha}(\mathbf{s}) - \psi^{\alpha}(\mathbf{r}^*)) \right) \cdot \mathbf{n} \\ \mp \nabla \psi^{\alpha} \cdot \mathbf{n}(\mathbf{r}^*) \left(\frac{1}{2\pi} \oiint_{\Gamma} \frac{\mathrm{d}\Gamma}{|\mathbf{r}^* - \mathbf{s}|} \right) = 0.\end{aligned} \tag{33}$$

As a consequence of Green's second identity, observe that this expression holds for any harmonic function $\psi^{\alpha} = \pm\eta$ such that $\nabla^2 \eta = 0$, and hence,

$$\begin{aligned}S(\mathbf{r}^*) &\equiv \frac{1}{2\pi} \oiint_{\Gamma} \frac{\mathrm{d}\Gamma}{|\mathbf{r}^* - \mathbf{s}|} \\ &= \frac{1}{\nabla \eta \cdot \mathbf{n}(\mathbf{r}^*)} \left[\eta(\mathbf{r}^*) + \frac{1}{2\pi} \oiint_{\Gamma} \mathrm{d}\Gamma \left(\eta(\mathbf{s}) \nabla \left(\frac{1}{|\mathbf{r}^* - \mathbf{s}|} \right) + \frac{1}{|\mathbf{r}^* - \mathbf{s}|} \nabla (\eta(\mathbf{r}^*) - \eta(\mathbf{s})) \right) \cdot \mathbf{n} \right].\end{aligned} \tag{34}$$

In particular, taking the simple quadratic form,

$$\eta(x, y, z) = \frac{1}{2}(x^2 + y^2) - z^2, \tag{35}$$

allows the singular integral S to be easily computed.

3.2. Mesh generation and spatial resolution

A three-dimensional geodesic mesh was generated using a commercial graphics package [31] to triangulate the surface with nodes falling exactly on the parametrically defined Γ. As well as setting linear dimensions, the package also permits flexible specification of node density in each direction and supports the ASCII Scene Export (ASE) format for node coordinates and mesh connectivity. A PERL script was created, operating on ASE input, to calculate surface element centroids, areas and unit normals for submission to the boundary integral program.

Although Maxwell's theory requires the *total* electrostatic potential Φ to be continuous across the dielectric boundary, the direct Coulomb ϕ_{C} and reaction field ψ components will generally exhibit jump discontinuities on Γ. A consequence of discretising the smooth surface Γ into a piecewise analytic set of polygons is to blur these discontinuities over a non-zero range. The effect is illustrated in Fig. 3, where the identity,

$$H(\mathbf{u}) \equiv -\frac{1}{4\pi} \oiint_{\Gamma} \mathrm{d}\Gamma_s \nabla \left(\frac{1}{|\mathbf{u} - \mathbf{v}|} \right) \cdot \mathbf{n} = \int_{\mathscr{B} \cup \Gamma_s} \mathrm{d}\mathbf{v} \delta(\mathbf{u} - \mathbf{v}) = \begin{cases} 1 & (\mathbf{u} \in \mathscr{B}), \\ 1/2 & (\mathbf{u} \in \Gamma_s), \\ 0 & (\mathbf{u} \notin (\mathscr{B} \cup \Gamma_s)) \end{cases} \tag{36}$$

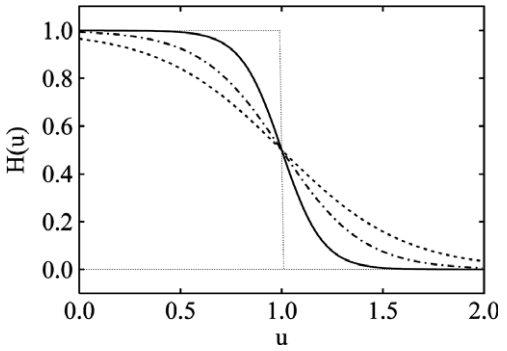

Fig. 3. An illustration of the effect of mesh approximations for smooth boundaries in the numerical implementation of the boundary integral method. As the number of mesh facets is increased the jump discontinuity is described more accurately. The results are shown here for a meshed unit sphere with 400 (– –); 600 (- · -); and 800 (——) facets, respectively.

is checked numerically on the unit ball $\mathscr{B} = \{\mathbf{u} : |\mathbf{u}| < 1\}$ bounded by the spherical surface $\Gamma_s : |\mathbf{u}| = 1$. As the mesh becomes increasingly coarse, the width of the transitional region grows where numerical estimates of field values are of relatively poor accuracy. In electrostatics applications, a specified precision on fields calculated at a given distance from the boundary provides a criterion on node density for mesh generation.

3.3. Discrete linear system

Given a piecewise analytic mesh of P plane polygonal faces, each with area $\mathscr{A}_p$ and associated with the point $\mathbf{r}^* \in \Gamma$ for $p = 1, \ldots, P$, that represents the closed surface Γ with sufficient accuracy, it is convenient to first define the mesh vectors,

$$v_p(\mathbf{r}) = \frac{\mathscr{A}_p}{4\pi} \frac{1}{|\mathbf{r}_p^* - \mathbf{r}|}, \quad v_p'(\mathbf{r}) = \frac{\mathscr{A}_p}{4\pi} \nabla \left(\frac{1}{|\mathbf{r}_p^* - \mathbf{r}|} \right) \cdot \mathbf{n}(\mathbf{r}_p^*) \tag{37}$$

and the traceless mesh matrices,

$$M_{pq} = \begin{cases} 0; & p = q, \\ 2v_q(\mathbf{r}_p^*); & p \neq q, \end{cases} \quad M'_{pq} = \begin{cases} 0; & p = q, \\ 2v'_q(\mathbf{r}_p^*); & p \neq q. \end{cases} \tag{38}$$

In common with most boundary element approaches described in the literature, the induced polarisation charge is supposed sufficiently slowly varying over the boundary, or the mesh is sufficiently dense, that the reaction field may be assumed constant on each element. Now, recall the discretised boundary conditions,

$$\begin{aligned} \psi_p^{\text{int}} - \psi_p^{\text{ext}} &= -\left(\phi_{\text{C}\,p}^{\text{int}} - \phi_{\text{C}\,p}^{\text{ext}} \right) \equiv -(\Delta\phi_{\text{C}})_p, \\ \varepsilon^{\text{int}} \left(\frac{\partial \psi^{\text{int}}}{\partial n} \right)_p - \varepsilon^{\text{ext}} \left(\frac{\partial \psi^{\text{ext}}}{\partial n} \right)_p &= -\left(\varepsilon^{\text{int}} \left(\frac{\partial \phi_{\text{C}}^{\text{int}}}{\partial n} \right)_p - \varepsilon^{\text{ext}} \left(\frac{\partial \phi_{\text{C}}^{\text{ext}}}{\partial n} \right)_p \right) \equiv -(\Delta D_{\text{C}})_p, \end{aligned} \tag{39}$$

and the boundary integral equations,

$$\begin{aligned} \psi_p^{\text{int}} + \sum_q \left\{ \psi_q^{\text{int}} M'_{pq} - M_{pq} \left(\frac{\partial \psi^{\text{int}}}{\partial n} \right)_q - \left(\frac{\partial \psi^{\text{int}}}{\partial n} \right)_p \right\} - S_p \left(\frac{\partial \psi^{\text{int}}}{\partial n} \right)_p &= 0, \\ \psi_p^{\text{ext}} - \sum_q \left\{ \psi_q^{\text{ext}} M'_{pq} - M_{pq} \left(\frac{\partial \psi^{\text{ext}}}{\partial n} \right)_q - \left(\frac{\partial \psi^{\text{ext}}}{\partial n} \right)_p \right\} + S_p \left(\frac{\partial \psi^{\text{ext}}}{\partial n} \right)_p &= 0 \end{aligned} \tag{40}$$

including the singular integral S_p on each mesh face. Introducing a further matrix that depends only on the boundary geometry,

$$G_{pq} = \delta_{pq} \sum_r M_{qr} - S_q \quad - M_{pq}, \tag{41}$$

the $4P \times 4P$ linear equation system can be represented in block matrix form,

$$\begin{Bmatrix} \mathbf{I} & 0 & -\mathbf{I} & 0 \\ 0 & \varepsilon^{\text{int}}\mathbf{I} & 0 & -\varepsilon^{\text{ext}}\mathbf{I} \\ (\mathbf{M}' + \mathbf{I}) & \mathbf{G} & 0 & 0 \\ 0 & 0 & (\mathbf{M}' - \mathbf{I}) & \mathbf{G} \end{Bmatrix} \begin{Bmatrix} \boldsymbol{\Psi}^{\text{int}} \\ \boldsymbol{\Psi}'^{\text{int}} \\ \boldsymbol{\Psi}^{\text{ext}} \\ \boldsymbol{\Psi}'^{\text{ext}} \end{Bmatrix} = \begin{Bmatrix} -\Delta\boldsymbol{\Phi}_{\text{C}} \\ -\Delta\mathbf{D}_{\text{C}} \\ 0 \\ 0 \end{Bmatrix}. \tag{42}$$

Elementary row operations render an upper triangular form and backsubstitution directly yields the solutions,

$$\begin{aligned} \boldsymbol{\Psi}^{\text{int}} &= \tfrac{1}{2\bar{\varepsilon}}\mathbf{J}(\varepsilon^{\text{ext}}\mathbf{K}^{\text{ext}}\Delta\boldsymbol{\Phi}_{\text{C}} + \Delta\mathbf{D}_{\text{C}}), \ \boldsymbol{\Psi}'^{\text{int}} = -\mathbf{K}^{\text{int}}\boldsymbol{\Psi}^{\text{int}}, \\ \boldsymbol{\Psi}^{\text{ext}} &= \tfrac{1}{2\bar{\varepsilon}}\mathbf{J}\ \varepsilon^{\text{int}}\mathbf{K}^{\text{int}}\Delta\boldsymbol{\Phi}_{\text{C}} + \Delta\mathbf{D}_{\text{C}}), \ \boldsymbol{\Psi}'^{\text{ext}} = -\mathbf{K}^{\text{ext}}\boldsymbol{\Psi}^{\text{ext}}, \end{aligned} \tag{43}$$

where

$$\mathbf{J} = (\mathbf{G}^{-1}(\mathbf{I} - \Upsilon_{\varepsilon}\mathbf{M}'))^{-1}, \quad \mathbf{K}^{\text{int}} = \mathbf{G}^{-1}(\mathbf{M}' + \mathbf{I}), \quad \mathbf{K}^{\text{ext}} = \mathbf{G}^{-1}(\mathbf{M}' - \mathbf{I}). \tag{44}$$

In the event that $\mathbf{M}'$ is nilpotent, then $\mathbf{J}$ may be expanded as a finite geometric series reminiscent of the effective image representations of the canonical geometries discussed in Section 2.1,

$$\exists n \in \mathbb{N} : \mathbf{M}'^{n} = 0 \quad \Rightarrow \quad \mathbf{J} = \sum_{k=0}^{n} (\Upsilon_{\varepsilon}\mathbf{M}')^{k} \quad \mathbf{G}. \tag{45}$$

The reaction field anywhere can be finally computed as the sum of two P-order scalar products,

$$\psi^{\text{int}}(\mathbf{r}) = \boldsymbol{\Psi}'^{\text{int}} \cdot \mathbf{v}(\mathbf{r}) - \boldsymbol{\Psi}^{\text{int}} \cdot \mathbf{v}'(\mathbf{r}) \quad (\mathbf{r} \in \mathscr{D}), \tag{46}$$

$$\psi^{\text{ext}}(\mathbf{r}) = \boldsymbol{\Psi}^{\text{ext}} \cdot \mathbf{v}'(\mathbf{r}) - \boldsymbol{\Psi}'^{\text{ext}} \cdot \mathbf{v}(\mathbf{r}) \quad (\mathbf{r} \in \overline{\mathscr{D}}), \tag{47}$$

where the vectors $\boldsymbol{\Psi}$ and $\boldsymbol{\Psi}'$ depend only on the Γ-mesh and need be evaluated once only for a fixed boundary.

3.4. Multiple disjoint boundaries

As well as handling arbitrarily shaped smooth interfaces, a second important advantage of the boundary integral formulation is the easy extension to describe any collection of disjoint boundaries. In particular, consider a contour of the form,

$$\Gamma = \lim_{\delta \to 0} \quad \Gamma_0 + \sum_{m=1}^{N_d} (\Gamma_m + \Omega_m(\delta)) \quad , \tag{48}$$

where each of the N_d domains is bounded by a surface Γ_m, that is also connected by a tube $\Omega_m(\delta)$ of diameter δ to its predecessor Γ_{m-1}. For two domains, the composite contour Γ is illustrated in Fig. 4. In the limit of small δ and taking the surface Γ_0 to infinity, Green's second identity again affords Eq. (31) for the external reaction potential as before, while a similar result is obtained for the internal field on each domain,

Table 1
Typical CPU usage for solving the discrete linear system of field equations on a spherical mesh with P boundary elements giving a resolution χ (Eq. (51)) in the geometry of Fig. 1(b)

k	P_k	χ	τ_k^{mat}/s	R_k^{mat}	$\tau_k^{\mathrm{pot}}(N)$/s			R_k^{pot}	κ_{G}	κ_{M}
					$N=1$	$N=40$	$N=100$			
1	54	2.42	1.43	–	2.11	2.54	3.01	–		
2	88	3.94	2.00	0.69	3.11	3.81	4.60	0.80	4.54	3.55
3	130	5.81	5.17	2.43	4.49	5.76	6.01	0.94	3.90	3.48
4	180	8.06	11.81	2.54	6.39	7.61	8.78	1.08	3.31	3.44
5	238	10.7	29.32	3.26	9.20	10.38	12.79	1.30	2.42	3.38
6	304	13.6	65.70	3.30	11.74	13.55	16.08	1.00	2.02	3.34
7	360	16.1	85.86	1.58	12.81	14.88	17.43	0.52	1.81	3.33
8	550	24.6	284.35	2.83	18.62	23.78	27.12	0.89	1.62	3.32
9	840	37.6	978.13	2.92	32.86	38.20	44.44	1.33	1.45	3.32
10	1520	68.0	5743.99	2.98	54.43	69.02	76.92	0.86	1.45	3.31

A single unit internal charge $N^{\mathrm{int}}=1$ is placed at $(a/4,0)$ and the dielectric ratio is $\varepsilon^{\mathrm{int}}{:}\varepsilon^{\mathrm{ext}}=40{:}80$. The time τ^{mat} for computing the solution vectors (Eq. (43)) is compared with the time $\tau^{\mathrm{pot}}(N)$ for 1000 total potential evaluations given a configuration of $N^{\mathrm{ext}}=N-N^{\mathrm{int}}$ unit external charges randomly located in the concentric spherical shell $2\leqslant r/a\leqslant 5$. Complexity scaling factors are defined by $R_k^{\mathrm{mat}}=\ln(\tau_k^{\mathrm{mat}}/\tau_{k-1}^{\mathrm{mat}})/\ln(P_k/P_{k-1})$ and $R_k^{\mathrm{pot}}=\ln((\tau_k^{\mathrm{pot}}(N)+N\tau_k^{\mathrm{pot}}(1))/(\tau_{k-1}^{\mathrm{pot}}(N)+N\tau_{k-1}^{\mathrm{pot}}(1)))/\ln(P_k/P_{k-1})$. Scaling with mesh resolution indicates the expected P^3 behaviour of the one-off τ^{mat} cost, that is dominated by matrix inversion processes, while τ^{pot} is essentially linear in both P and N. The calculations were performed on a P3 2GHz processor running Ubuntu Breezy with the algorithm written in Python (http://www.python.org). Condition numbers κ_{G} and κ_{M} for the matrices $\mathbf{G}$ and $\mathbf{I}-{}_{\varepsilon}\mathbf{M}'$, respectively, are also reported for the discrete representation of the dielectric boundary.

4.2. Canonical geometries

As a consequence of applying Green's theorem only to the reaction field instead of the total potential, numerical "smoothing" (Section 3.2) of the discontinuity in ψ at the boundary gives rise to an apparent jump in Φ. It must be emphasised that this does *not* constitute a breach of the electrostatic boundary conditions, which are explicitly respected by the formulation, but is simply a computational error associated with the finite discrete representation of the surface. In principle, the error can be systematically reduced to an arbitrarily small value by sufficiently increasing the mesh resolution. The plane geometry (Fig. 1(a)) provides the natural test bed for analysing this behaviour.

Fig. 5 compares analytic and numerical results for the total potential, relative to bare Coulomb field, as a function of distance from the dielectric boundary with $\varepsilon^{\mathrm{int}}=2$ and $\varepsilon^{\mathrm{ext}}=80$ that may be considered as extreme values appropriate for proteins in aqueous solution at ambient temperature. This infinite surface is represented by a finite square sheet of dimensions $30d\times 30d$ or a disk of radius $15d$ with the assumption that contributions to the boundary integral are negligible beyond this range. In the context of fluid dynamics with free surface flows, Grandison and Vanden-Broeck [32] have demonstrated the validity of analogous truncation schemes and discussed techniques for taking edge effects into account. For a total meshed area $\mathscr{A}=\sum_{p=1}^{P}\mathscr{A}_p$ of P elements and a characteristic charge-surface separation d, the grid resolution is quantified by the parameter,

$$\chi=\frac{Pd^2}{\mathscr{A}}. \tag{51}$$

As the boundary is approached, the numerical estimates $\tilde{\psi}$ of the reaction fields behave like,

$$\lim_{z\to 0^+}\tilde{\psi}^{\mathrm{int}}(0,z)=\lim_{z\to 0^+}\tilde{\psi}^{\mathrm{ext}}(0,-z)=\frac{1}{2}\lim_{z\to 0^+}\left(\psi^{\mathrm{int}}(0,z)+\psi^{\mathrm{ext}}(0,-z)\right), \tag{52}$$

which therefore leads to,

$$\lim_{z\to 0^+}\left(\tilde{\Phi}^{\mathrm{int}}(0,z)-\tilde{\Phi}^{\mathrm{ext}}(0,-z)\right)=\lim_{z\to 0^+}\left(\phi_{\mathrm{C}}^{\mathrm{int}}(0,z)+\tilde{\psi}^{\mathrm{int}}(0,z)-\tilde{\Phi}^{\mathrm{ext}}(0,-z)\right)=\lim_{z\to 0^+}\phi_{\mathrm{C}}^{\mathrm{int}}(0,z), \tag{53}$$

so that the calculated total field exhibits an apparent jump equal to $\phi_{\mathrm{C}}(0,0^+)$ at the boundary as confirmed by Fig. 5. In general, this hiatus will correspond to the discontinuity in Coulomb fields at the interface,

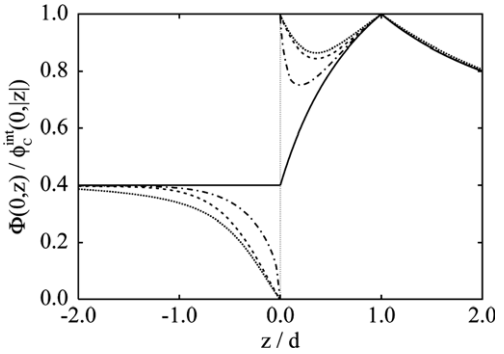

Fig. 5. Total reduced potential field generated by a single unit charge located at $(0,d)$ in a planar geometry. Analytic calculations (full lines) are compared with numerical results obtained by the boundary integral scheme (broken lines) with varying mesh resolutions $\chi = 0.89$ $(\cdots)$, $\chi = 2.00$ $(- -)$ and $\chi = 2.92$ $(- \cdot -)$.

$$\lim_{\mathbf{r}\to\mathbf{r}^*} \phi_C^{\text{int}}(\mathbf{r}) - \lim_{\mathbf{r}'\to\mathbf{r}^*} \phi_C^{\text{ext}}(\mathbf{r}') \quad \text{where } \mathbf{r} \in \mathscr{D},\ \mathbf{r}' \in \overline{\mathscr{D}},\ \mathbf{r}^* \in \Gamma. \tag{54}$$

As also indicated in Fig. 5, however, the extent to which this error propagates into the adjoining domains can be effectively controlled by assigning a sufficiently high mesh resolution χ. Moreover, for field points remote from the boundary, the agreement between numerical and analytic calculations is excellent.

For the applications with statistical mechanical simulations that we envisage, the closest approach distance to a dielectric boundary is often known *a priori* and the required mesh granularity can be pre-determined. In many cases, however, this might present an unacceptably high computational cost or, more significantly, the potential field may need to be resolved arbitrarily close to the boundary in order to capture the features of interest. It is natural in such situations to remove any boundary jumps by invoking some smooth interpolation scheme. To test the feasibility of this approach, we consider the simplest linear interpolation of the form

$$\Phi(\mathbf{r}) = \Phi^{\text{int}}(\mathbf{s} - \xi\mathbf{n}(\mathbf{s})) + \frac{1}{2}\left(1 \pm \frac{|\mathbf{r}-\mathbf{s}|}{\xi}\right)(\Phi^{\text{ext}}(\mathbf{s} + \xi\mathbf{n}(\mathbf{s})) - \Phi^{\text{int}}(\mathbf{s} - \xi\mathbf{n}(\mathbf{s}))), \tag{55}$$

where $\mathbf{s} \in \Gamma$ is the solution of $(\mathbf{r}-\mathbf{s})\cdot\mathbf{n}(\mathbf{s}) = |\mathbf{r}-\mathbf{s}|$ and ξ is a fixed range parameter. The positive sign is taken for $\mathbf{r} \in \overline{\mathscr{D}}$, and the negative sign for $\mathbf{r} \in \mathscr{D}$. For the spherical geometry (Fig. 1(b)), with a single unit charge located at $(a/4, 0)$ in the interior dielectric of relative permittivity $\varepsilon^{\text{int}} = 40$ (and $\varepsilon^{\text{ext}} = 80$), typical results of this interpolation scheme are illustrated in Fig. 6 by comparing the total potential field obtained from the boundary integral method with analytic calculations. At low mesh resolution $\chi = 2.42$, similar to that of the planar examples, the relative error is typically less than 1% within each domain, but rises to a peak value around 10% on the boundary at the centre of the interpolation region. With increasing resolution, however, the

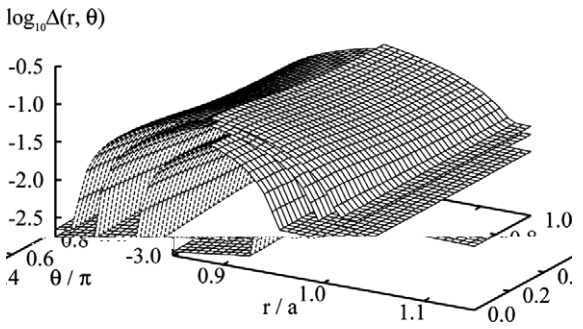

Fig. 6. The relative error in total electrostatic potential of the numerical scheme compared to the analytic result $\Delta(r,\theta) = |\tilde{\Phi}(r,\theta)/\Phi(r,\theta) - 1|$ for a spherical boundary of radius a enclosing a single unit charge located at $(a/4, 0)$. Three increasingly fine mesh densities are indicated corresponding to χ values of 2.42, 13.6 and 68.0 that yield respectively smaller overall errors.

interpolation range ξ can be decreased with a concomitant systematic reduction in error throughout. For this particular configuration, the partition of the total field with an exact treatment of the interior Coulomb contribution is again evident in the smaller error associated with the low dielectric domain. As well as increasing precision by refining the mesh resolution, higher order interpolation schemes would also offer computationally cheap improvement.

In the cylindrical geometry (Fig. 1(c)), with unit charge located at $(a/4, 0, 0)$, results from a treatment of the equivalent dielectric model (ε^{int}:$\varepsilon^{\text{ext}} = 40{:}80$) are shown in Figs. 7 and 8. At a mesh resolution of $\chi = 13.1$, and with the same triangulation previously used in our study of B-DNA [16], the total potential field obtained by the boundary integral method is in excellent agreement with the analytic calculations in both domains (Fig. 7). This is confirmed in Fig. 8 where a section through the dielectric boundary also demonstrates the effectiveness of the linear interpolation scheme in eliminating the jump artefact.

4.3. Glycinin homohexamer: a toy model

As a major class of seed storage proteins, globulins from various legumes and tree nuts are important feed stock sources for animal husbandry as well as being significant direct contributors to the human diet. Within the cupin superfamily, the 11S globulins are hexamers of heteroligomeric subunits, each comprising an acidic and a basic polypeptide linked through a disulphide bond, and exhibiting the distinctive "jelly-roll" or "double-stranded β-helix" dolioform structure characteristic of the class. Alongside its nutritional value, glycinin (the 11S globulin derived from soya) has been confirmed as an allergen in common with several other cupins [33]. Following synthesis of the constituent subunits in the cell, a proglycinin trimer of plane triangular symmetry is formed before a specific post-translational cleavage triggers assembly of the mature glycinin hexamer.

The proglycinin homotrimer of A1aB1b subunits has been successfully crystallised to yield an X-ray structure that fixes about 78% of the residues, with the remainder accounted for by six disordered loops closely matching variable regions of the primary sequence among other 11S globulins [34]. From these coordinates (Brookhaven Protein Data Bank file 1FXZ), we have constructed a very naive electrostatic model by assigning $+1$ and $+\frac{1}{2}$ charges to the terminal nitrogen atoms of lysine residues and guanidino groups of arginine side chains, respectively, while $-\frac{1}{2}$ partial charges are located on each carboxylic oxygen atom of aspartate and glutamate residues. The small number of histidine residues (five per subunit) are considered un-ionised. In total then, the homotrimer comprises $N = 348$ charges ζ_i, located at $\mathbf{r}_i$, that endow an overall valency of $Q = +6$. Again for the sake of simplicity, atomic detail of the dielectric boundary is eschewed in favour of a ring torus enclosing all the charges but only roughly approximating the symmetry and spatial extent of the trimer as indicated in Fig. 9. The torus dimensions are characterised by a wheel radius $R_{\text{w}} = 27.5$ Å and a tube radius $R_{\text{t}} = 23.5$ Å. A mesh of 832 facets is generated that, with a single charge positioned at

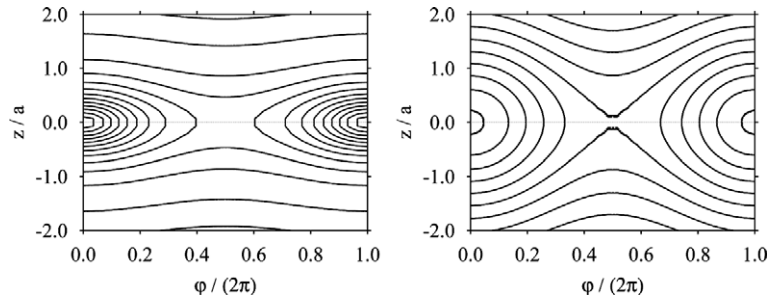

Fig. 7. Projections of the reduced electrostatic potential field $\Phi(\rho, \varphi, z)/\phi_C^{\text{int}}(0,0,0)$ generated by a single unit charge located at $(a-d, 0, 0)$ in a cylindrical geometry with barrel radius a and charge-boundary separation $d = 3a/4$. Analytic calculations (full lines) are compared with numerical results obtained by the boundary integral scheme (broken lines) with a mesh resolution of $\chi = 31.1$. On the scale of the figure, the data are essentially coincident. Panel (a) shows the cylindrical sheet at $\rho = a - d/2$ in the interior domain, with relative dielectric permittivity $\varepsilon^{\text{int}} = 40$. Contour levels increase towards the charge singularity as follows: $0.75, 1.0, 1.5, \ldots, 6.5$. Panel (b) shows corresponding results for $\rho = 2a$ in the exterior domain with $\varepsilon^{\text{ext}} = 80$ and contour levels at $0.55, 0.60, \ldots, 0.95$.

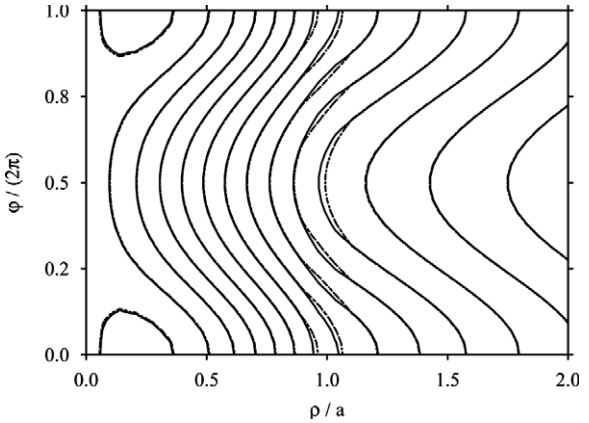

Fig. 8. Comparison of analytic (full lines) and numerical (broken lines) results for the reduced electrostatic potential field in the cylindrical geometry as described in Fig. 7. A plane section perpendicular to the cylinder axis ($z = a$) of the function $\Phi(\rho, \varphi, z)/\phi_{\mathrm{C}}^{\mathrm{int}}(0, 0, 0)$ is shown, with contour levels at $2.0, 1.9, \ldots, 0.7$ decreasing from the charge singularity on the left of the plot.

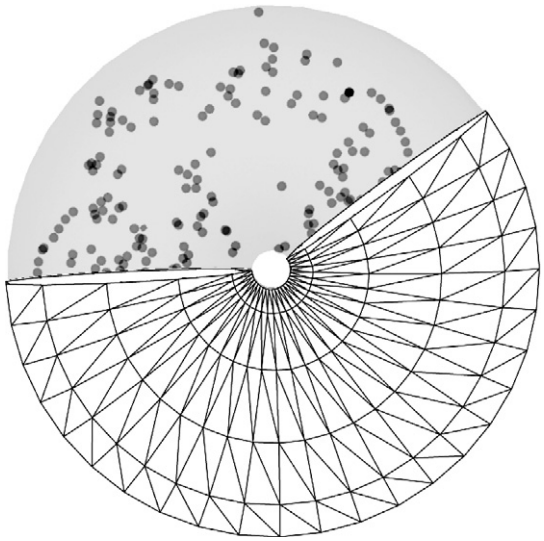

Fig. 9. A schematic representation of the proglycinin homotrimer model viewed in the equatorial plane perpendicular to the threefold symmetry axis. The charge configuration of a single subunit is explicitly indicated and overlaid with a portion of the toroidal mesh corresponding to the dielectric boundary.

$d = \frac{3}{4}R_{\mathrm{t}}$ giving $\chi = 10.1$, provides a resolution similar to the cylindrical geometry discussed above and suggesting comparable accuracy in potential field estimates.

The application of this model to predict the likely relative orientation θ for the ground state of the mature glycinin hexamer is not only of some biological interest, but also provides an elegant test of the boundary integral formulation for multiple disjoint domains. By aligning two copies, denoted A and B, of the proglycinin model along a common axis with a centre-to-centre separation h, we neglect thermal contributions and consider only the electrostatic energy of such a configuration,

$$U_{\mathrm{gly}}(\theta, h) = \frac{1}{2}\sum_{i=1}^{N} \zeta_i^{(\mathrm{A})} \Phi(\mathbf{r}_i^{(\mathrm{A})}(\theta, h)) + \frac{1}{2}\sum_{j=1}^{N} \zeta_j^{(\mathrm{B})} \Phi(\mathbf{r}_j^{(\mathrm{B})}(\theta, h)). \tag{56}$$

A convenient normalisation is obtained from the energy of two infinite parallel plates each carrying a uniform surface charge density equivalent to the total proglycinin charge Q projected onto the equatorial annulus of area $\mathscr{A}_\alpha$,

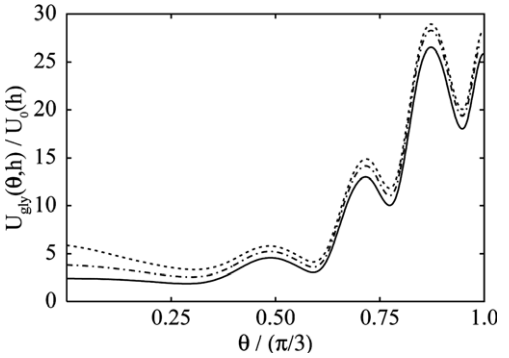

Fig. 10. The electrostatic energy $U_{\mathrm{gly}}(\theta,h)$ of two coaxial and parallel proglycinin homotrimers at centre-centre separation h as a function of relative orientation angle θ. Primitive model (PM) results (——), with entirely uniform relative permittivity ($\varepsilon^{\mathrm{int}} = \varepsilon^{\mathrm{ext}} = 80$), are compared with a "barbarous" inhomogeneous dielectric model (BM) (- - -) ($\varepsilon^{\mathrm{int}}$:$\varepsilon^{\mathrm{ext}} = 2{:}80$) at separation $h/(2R_{\mathrm{t}}) - 1 = 0.106$. The corresponding BM results at separation $h/(2R_{\mathrm{t}}) - 1 = 0.160$ are also shown (- · -). In each case, $U_{\mathrm{gly}}(\theta,h)$ is normalised by the electrostatic energy $U_0(h)$ of infinite parallel planes carrying an equivalent uniform surface charge density at separation h.

$$U_0(h) = \frac{Q^2 h}{2\epsilon_0 \varepsilon^{\mathrm{ext}} \mathscr{A}_\alpha} = \frac{Q^2 h}{8\pi\epsilon_0 \varepsilon^{\mathrm{ext}} R_{\mathrm{w}} R_{\mathrm{t}}}. \tag{57}$$

Owing to the axial symmetry of the boundary tori, the matrix inversion steps are required only once. Thus, the dependence of the hexamer energy on the relative orientation of proglycinin charge distributions can be obtained cheaply with high angular resolution. Fig. 10 compares calculations of U_{gly} in the primitive model (PM), with entirely uniform relative permittivity ($\varepsilon^{\mathrm{int}} = \varepsilon^{\mathrm{ext}} = 80$) against a "barbarous" inhomogeneous dielectric model (BM) with $\varepsilon^{\mathrm{int}}$:$\varepsilon^{\mathrm{ext}} = 2{:}80$ that is often invoked for the description of aqueous protein solutions [16]. At a separation $h/(2R_{\mathrm{t}}) - 1 = 0.106$, the PM predicts a lower energy for all orientations, but with a somewhat shallower basin around the eclipsed ($\theta = 0$) configuration. This trend is also followed by the BM but at larger separation $h/(2R_{\mathrm{t}}) - 1 = 0.160$. Certainly, all the calculations indicate that the eclipsed states are very strongly favoured over staggered arrangements ($\theta = \pi/3$), though there are also significant local minima at intermediate orientations that could possibly support non-equilibrium jammed structures. These very preliminary results also suggest that an absolute minimum energy may well be achieved exactly at $\theta = 0$ but at somewhat larger separation.

Adachi and coworkers [35] have recently verified that the glycinin homohexamer does indeed adopt the eclipsed configuration in the crystalline state. Although the agreement with our simple electrostatic model supports the hypothesis that direct charge interactions play important roles for the stability of the hexamer and in the assembly process, it is clear that other phenomena must also be involved. In particular, the experimental evidence [35] implicates two nearby highly charged disordered loops on each proglycinin subunit, together accounting for 66/105 of the delocalised residues with some 44% ionised (compared with around 18% for the X-ray visible regions), in a face-to-face stacking mechanism that buries and protects the interchain disulfide linkage on hexamer formation. The correlated dynamical aspects of this operation are the province of the statistical mechanical problem, but the basic force and/or energy calculations available from the present boundary integral formulation can be practically incorporated into a relevant simulation algorithm [16]. It is not difficult to imagine extensions of the naive electrostatic model to include mobile, but grafted polyelectrolyte chains representing the disordered loops.

5. Discussion

In this paper, a new boundary integral formulation is presented for electrostatic models comprising piecewise uniform dielectric continua. Significant improvements in numerical stability are achieved over alternative schemes by partitioning the total electrostatic potential, treating direct Coulomb contributions exactly and applying Green's theorem only to the residual reaction field. Despite observing the electrostatic boundary conditions, this procedure introduces an interfacial jump since the smoothing of the reaction potential

discontinuity is not reflected in the Coulomb part. Nevertheless, detailed examination in the three canonical geometries of plane, sphere and circular cylinder where analytic solutions exist, demonstrates that simple interpolation near the boundary allied with a mesh of sufficiently high resolution can effectively eliminate this artefact. For the cylindrical case, an analytic ''image'' charge expansion is obtained, as an incidental result, that complements corresponding well-known series for the planar and spherical geometries. This unification exemplifies the general ''multiple induction expansion'' proposed by Shaw.

A relevant biomolecular application is also considered by developing a naive electrostatic model for the proglycinin trimer, a storage protein aggregate from soybean, and estimating the ground state orientation of the corresponding hexameric glycinin complex. As well as testing the boundary integral formulation for a pair of disjoint dielectric domains, this configuration also confirms that the scheme is equally robust for compact surfaces of non-trivial genus. Notwithstanding the simplicity of the model, the predicted ground state structure is consistent with experimental observation.

For studies of biomolecular association, an apparent disadvantage of the boundary element method lies in the need to compute expensive matrix inversions whenever a dielectric interface is distorted; either by significant local conformational change of single molecules, or by global configurational re-organisation of many, or by a combination of both effects. Since the piecewise uniform dielectric continuum picture arises from the idea of effective interactions averaged over secondary degrees of freedom, we have previously promulgated [16] the hypothesis that appropriate dielectric boundaries may not be exclusively determined by short-ranged geometric constraints, but should also recognise effects from the electrostatic environment including charge and dipole distributions. It then follows that an effective description in terms of a macroscopic dielectric response may not be especially sensitive to small conformational re-arrangements. The same argument supports the view that an optimal dielectric boundary may be significantly more smooth than the geometric envelope of constituent atoms, thereby relaxing the criteria on mesh resolution and easing the technical difficulties of grid construction. On the other hand, it seems probable that small boundary deformations, relevant for dynamical simulations, could be accommodated by a low order perturbative scheme that approximates the effects on electrostatic fields without resorting to complete matrix inversions. Indeed, owing to the essential linearity of the electrostatic problem, Zhou [8] has shown that such a device is possible for biomolecular interactions with multiple bounded domains where the collective effects of configurational change can be simply expressed in terms of each individual molecular surface, with their attendant mesh matrix inverses computed once only.

Further developments will consider a differentiably smooth boundary with curvilinear elements applied to a more realistic molecular surface. In particular, refinement of the glycinin model to also include the dynamical effects of the disordered charge bearing loops will need to address the statistical mechanical problem. With the present boundary integral method for fast evaluation of electrostatic energies and forces, both MC and MD simulations of such a model appear to be entirely tractable.

Acknowledgments

RP is supported by the core strategic grant of the UK Biotechnology and Biological Sciences Research Council. We are grateful to the reviewers for alerting us to a number of useful complementary articles.

References

[1] N. Sinha, S.J. Smith-Gill, Curr. Protein Peptide Sci. 3 (2002) 601.
[2] D.L. Beveridge, K.J. McConnell, Curr. Opin. Struct. Biol. 10 (2000) 182.
[3] J. Warwicker, H.C. Watson, J. Mol. Biol. 157 (1982) 671.
[4] M.E. Davis, J.A. McCammon, J. Comp. Chem. 10 (1989) 386.
[5] M. Holst, F. Saied, J. Comp. Chem. 14 (1993) 105.
[6] (a) M. Holst, N. Baker, F. Wang, J. Comp. Chem. 21 (2000) 1319;
(b) N. Baker, M. Holst, F. Wang, J. Comp. Chem. 21 (2000) 1343.
[7] A.H. Boschitsch, M.O. Fenley, H.-X. Zhou, J. Phys. Chem. B 106 (2002) 2741.
[8] H.-X. Zhou, Biophys. J. 65 (1993) 955.
[9] E.N.C. Mills, N. Marigheto, N. Wellner, S.A. Fairhurst, J.A. Jenkins, R. Mann, P.S. Belton, Biochim. Biophys. Acta 1648 (2003) 105.
[10] (a) R.J. Zauhar, R.S. Morgan, J. Mol. Biol. 186 (1985) 815;
(b) R.J. Zauhar, R.S. Morgan, J. Comp. Chem. 9 (1988) 171.

[11] (a) N.S. Goel, F. Gang, Z. Ko, J. Comp. Phys. 118 (1995) 172;
(b) N.S. Goel, Z. Ko, F. Gang, J. Comp. Phys. 118 (1995) 180.
[12] (a) B.J. Yoon, A.M. Lenhoff, J. Comp. Chem. 11 (1990) 1080;
(b) B.J. Yoon, A.M. Lenhoff, J. Phys. Chem. 96 (1992) 3130.
[13] (a) A.H. Juffer, E.F.F. Botta, B.A.M. van Keulen, A. van der Ploeg, H.J.C. Berendsen, J. Comp. Phys. 97 (1991) 144;
(b) A.H. Juffer, P. Argos, H.J. Vogel, J. Phys. Chem. B 101 (1997) 7664.
[14] J. Liang, S. Subramaniam, Biophys. J. 73 (1997) 1830.
[15] (a) B. Lu, D. Zhang, J.A. McCammon, J. Chem. Phys. 122 (2005) 214102;
(b) B. Lu, X. Cheng, T. Hou, J.A. McCammon, J. Chem. Phys. 123 (2005) 084904.
[16] S. Grandison, R. Penfold, J.-M. Vanden-Broeck, Chem. Phys. Phys. Chem. 7 (2005) 3486.
[17] F. Chen, D.M. Chipman, J. Chem. Phys. 119 (2003) 10289.
[18] R.G. Barrera, O. Guzmán, B. Balaguer, Am. J. Phys. 46 (1978) 1172.
[19] H.L. Friedman, Mol. Phys. 29 (1975) 1533.
[20] (a) P.B. Shaw, Phys. Rev. A 32 (1985) 2476;
(b) P.B. Shaw, Phys. Rev. A 35 (1987) 2254.
[21] J.D. Jackson, Classical Electrodynamics, third ed., John Wiley & Sons, New York, 1999.
[22] P. Linse, J. Phys. Chem. 90 (1986) 6821.
[23] R. Messina, J. Chem. Phys. 117 (2002) 11062.
[24] D. Hochberg, T.W. Kephart, G. Edwards, Phys. Rev. E 49 (1994) 851.
[25] R. Penfold, J.-M. Vanden-Broeck, S. Grandison, Integral Trans. Spec. Funct., in press, doi:10.1080/10652460601041219.
[26] C.M. Joshi, S.K. Bissu, J. Austral. Math. Soc. A 50 (1991) 333.
[27] C.J.F. Böttcher, second ed.Theory of Electric Polarization, vol. 1, Elsevier, Amsterdam, 1973.
[28] J.G. Kirkwood, J. Chem. Phys. 7 (1934) 351.
[29] H.-X. Zhou, Biophys. J. 64 (1993) 1711.
[30] E. Parau, J.-M. Vanden-Broeck, Euro. J. Mech. B 21 (2002) 643.
[31] 3D Studio Max, Version 3, Autodesk Inc., Montreal.
[32] S. Grandison, J.-M. Vanden-Broeck, J. Eng. Math. 54 (2006) 89.
[33] E.N.C. Mills, J. Jenkins, N. Marigheto, P.S. Belton, A.P. Gunning, V.J. Morris, Biochem. Soc. Trans. 30 (2002) 925.
[34] M. Adachi, Y. Takenaka, A.B. Gidamis, B. Mikami, S. Utsumi, J. Mol. Biol. 305 (2001) 291.
[35] M. Adachi, J. Kanamori, T. Masuda, K. Yagasaki, K. Kitamura, B. Mikami, S. Utsumi, Proc. Natl. Acad. Sci. 100 (2003) 7395.